AGU PUBLICATIONS

JGR

Journal of Geophysical Research: Planets

RESEARCH ARTICLE
10.1002/2015JE004830

**Key Points:**
- As revealed by SHARAD, Planum Boreum's basal unit is morphologically complex
- No climate change evidence found from the upper basal unit to the modern regime
- Regional wind, local climate, and ice armoring dictate accumulation patterns

**Correspondence to:**
T. C. Brothers,
TCBrothers@utexas.edu

**Citation:**
Brothers, T. C., J. W. Holt, and A. Spiga (2015), Planum Boreum basal unit topography, Mars: Irregularities and insights from SHARAD, *J. Geophys. Res. Planets*, *120*, 1357–1375, doi:10.1002/2015JE004830.

Received 14 APR 2015
Accepted 30 JUN 2015
Accepted article online 3 JUL 2015
Published online 31 JUL 2015



# Planum Boreum basal unit topography, Mars: Irregularities and insights from SHARAD

**T. C. Brothers[1], J. W. Holt[1], and A. Spiga[2]**

[1]University of Texas Institute for Geophysics, Jackson School of Geosciences, University of Texas, Austin, Texas, USA, [2]Laboratoire de Météorologie Dynamique, Université Pierre et Marie Curie, Paris, France

**Abstract** Shallow Radar investigations of Planum Boreum, Mars' "basal unit" (BU) deposit have revealed multiple reentrants, morphologic irregularities, and thickness trends that differ from those of the overlying north polar layered deposits. We present detailed subsurface maps for these features and offer explanation for genesis of the deposit's morphologic asymmetry, expressed in different erosional characteristics between 0°E–180°E and 180°E–360°E. Additionally, this work revealed a depression in the basal unit that may have provided a site for spiral trough initiation. Interpretations of the findings suggest that antecedent BU topography has a marked impact on modern morphology and that aeolian forces have been the dominant driver of polar deposit accumulation since at least the end of rupes unit emplacement. We find no results requiring explanation beyond common Martian surface processes, including aeolian erosion and impact armoring. To add to the detailed morphologic study of the BU, we mapped the variability of the BU radar reflection character. Combining generalized katabatic wind flow with the radar mapping results suggests that rupes unit material sourced the younger cavi. We present clear evidence that, while compositionally distinct from the overlying layered deposits, the BU and its morphology are intimately linked to the morphology of the north polar layered deposits. Combining geologic evidence with paleoclimate modeling, the deposits contain evidence for a long history of aeolian emplacement and modification.

## 1. Introduction

The "basal unit" (BU) is a low-albedo, sand and ice deposit on the north pole of Mars [*Malin and Edgett*, 2001; *Byrne and Murray*, 2002] that lies stratigraphically between the Vastitas Borealis Formation below and the relatively pure water ice north polar layered deposits (NPLD) above [*Tanaka et al.*, 2008; *Grima et al.*, 2009]. Here we use data from the Shallow Radar (SHARAD) on Mars Reconnaissance Orbiter to analyze the morphology and extent of the BU in order to better understand the deposit and its implications for climate. Where prior investigations focused on the homogeneity of BU material [*Byrne and Murray*, 2002; *Fishbaugh and Head*, 2005; *Selvans et al.*, 2010], this work concentrates on the inhomogeneity of this deposit to study depositional, and perhaps erosional, processes during and after BU growth. In addition, we also readdress the extent of BU material and present data supporting its continuity with Olympia Undae. Here we present the most detailed BU radar mapping to date including new, higher-resolution views of enigmatic features detected in an earlier SHARAD-based mapping effort [*Putzig et al.*, 2009].

This work also provides evidence that BU topography has affected the evolution of overlying ice material via aeolian processes. This supports the interpretations of *Howard* [2000] and recent discoveries that aeolian processes have played a critical role in the evolution of spiral troughs [*Smith and Holt*, 2010; *Smith et al.*, 2013], in the growth of Abalos Mensa [*Brothers et al.*, 2013], and likely in the long-term evolution of Chasma Boreale (Figure 1) [*Holt et al.*, 2010]. To illustrate how the change of topography between the BU epoch and the modern epoch impacts winds (and plausibly, the deposition of ice in early NPLD development), we used our new SHARAD map of the BU topography as an input for preliminary mesoscale atmospheric modeling.

## 2. Background

### 2.1. Visible Observations

An expansive deposit of low-albedo material beneath the NPLD of Mars was first revealed by Mars Orbiter Camera (MOC) [*Malin and Edgett*, 2001], and subsequent investigations indicated that this low-albedo

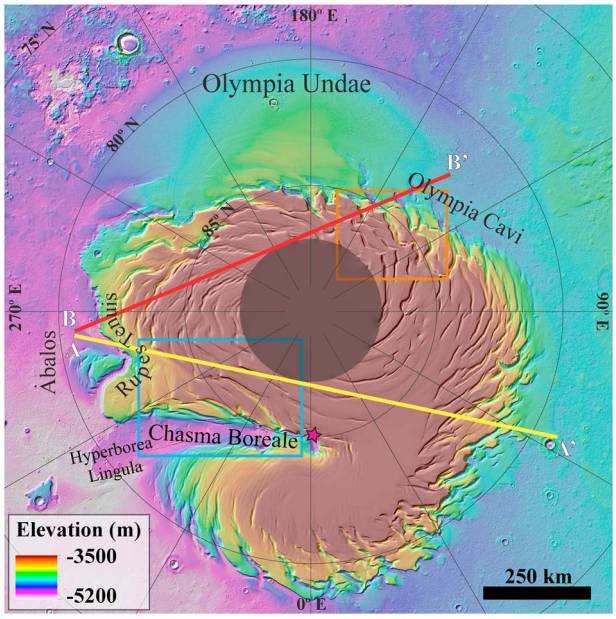


**Figure 1.** Color-shaded elevation map of modern Planum Boreum with location for radargrams in Figure 3 (yellow line, observation 804402000) and Figure 5 (red line, observation 521402000). The blue box is the location for Figures 13a and 13b, while the orange box is the location for Figures 13c and 13d. The magenta star in Chasma Boreale gives the location of Figure 2. Image is a combination of colorized MOLA topography with an overlain semitransparent shaded-relief image.

lithic- and ice-rich unit likely underlies most of the NPLD [*Byrne and Murray*, 2002; *Fishbaugh and Head*, 2005]. The material's low albedo, a stark contrast with the overlying high-albedo north polar layered deposit (NPLD) material, was the primary reason for its separation into a new geologic unit. The name basal unit (BU) [*Byrne and Murray*, 2002] derived from its stratigraphic position below the polar layered deposits and above the Vastitas Borealis unit.

The similarity of BU and circumpolar dune albedo spurred a hypothesis that the dune fields were sourced from the BU [*Byrne and Murray*, 2002]. This early hypothesis described the BU as a large, uniform mound of sand cemented by ice and posited that erosion of this deposit contributed to the circumpolar dune fields. In addition, it was posited that the sand material was deposited during an ancient climate regime different from the modern regime which favors deposition of water ice [*Byrne and Murray*, 2002]. Hence, the BU material may represent a different climate than the NPLD and is therefore significant in understanding polar ice processes.

While initial BU studies only offered a generalized extent of the deposit [*Byrne and Murray*, 2002], *Fishbaugh and Head* [2005] undertook detailed image-based mapping to further resolve the aerial extent of the BU deposit, making use of data from Mars Orbiter Camera (MOC) on Mars Global Surveyor. Their analyses indicated that BU underlay nearly all of Planum Boreum, the main exception being Gemina Lingula. *Fishbaugh and Head* [2005] also discovered that the BU is locally separated from the overlying NPLD material by an unconformity that is evident as both as an angular unconformity and disconformity. This demonstrated that the BU was distinct from the overlying NPLD and not simply a transition from dust-prevalent to dust-starved ice deposition.

Following the launch of Mars Reconnaissance Orbiter (MRO) in 2005, new data were available to the scientific community by late 2006. Included on this spacecraft was a new camera with resolution approximately 1 order of magnitude greater than narrow angle MOC images, the High Resolution Imaging Science Experiment (HiRISE) [*McEwen et al.*, 2007]. Making use of these high-resolution images, it became evident that more than one geologic unit is associated with the low-albedo material underlying the NPLD [*Herkenhoff et al.*, 2007; *Tanaka et al.*, 2008]. Optical mapping and careful unconformity delineation by *Tanaka et al.* [2008] divided the BU into two members, an older rupes unit and a younger Planum Boreum cavi unit (Figure 2).

The rupes unit has nearly planar bedding, a strong resistance to erosion, and can be found with outcrops exceeding 1 km thickness [*Tanaka et al.*, 2008]. In contrast, the cavi unit exhibits aeolian bedforms including cemented dunes and cross strata and is highly susceptible to modern erosion and slope failure [*Herkenhoff et al.*, 2007; *Russell et al.*, 2008; *Tanaka et al.*, 2008]. An unconformity with hundreds of meters of eroded material [*Tanaka et al.*, 2008] separates the two BU members. While the rupes unit appears markedly different from overlying NPLD, the cavi unit has a laterally transgressive contact with the NPLD [*Tanaka et al.*, 2008]. Perhaps more accurately, the contact between cavi and NPLD should be described as gradational with a compositional and morphologic change. The base of the cavi unit has concentrated sandy deposits; however, these sands transition from sand sheet to dune accumulation in the upper cavi. Upper cavi also contains alternating layers of relatively pure ice and sand, instead of the sand/ice mixture nearer the base. At the

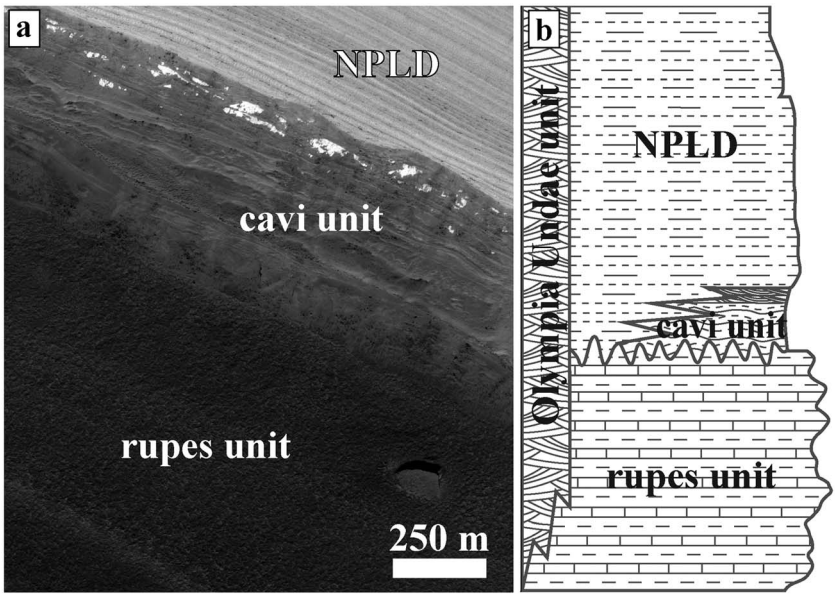


**Figure 2.** (a) HiRISE image ESP_0018975_2650 showing the stratigraphic units of this study. Uphill is to the right. (b) Simplified stratigraphic column modified from the work of *Tanaka et al.* [2008]. The two BU members (rupes unit and cavi unit) as well as the overlying north polar layered deposits are of primary interest.

top of the cavi unit the sand concentration lessens and there are examples of cemented dunes (Figure 3). The gradational contact between cavi unit and overlying NPLD indicates that the large unconformity separating the two BU members is not present between cavi and NPLD. It is likely that the largest depositional hiatus in Planum Boreum's extant volatile-rich material is the gap between rupes and cavi BU members.

### 2.2. Age

A maximum age of ~1 Ga (Early Amazonian) is estimated for the rupes unit based on geologic mapping and crater density [*Tanaka et al.*, 2008]. Rupes was therefore deposited during early, and perhaps middle, Amazonian Mars. The unconformity at the top of the rupes unit represents a depositional hiatus of unknown duration and means that the overlying cavi unit may be much younger. While younger than rupes unit, the cavi unit must be older than overlying NPLD based on the principle of superposition. During the past 5 Ma, Mars' mean obliquity has remained relatively low and close to that of today; however, prior to that, average obliquity was higher [*Laskar et al.*, 2004]. Ice growth models that incorporate orbital forcing are not able to accumulate lasting exposed ice reserves at the north pole prior to the obliquity shift ~5 Ma ago [*Levrard et al.*, 2007; *Greve et al.*, 2010]. This means that while the BU (at least the rupes unit) likely persisted for perhaps hundreds of million years, the overlying NPLD is likely younger than 5 Ma. The lithic material in the BU has likely helped to preserve its volatile content during periods of high obliquity. Similar armoring of presently unstable water ice reserves is observed with midlatitude glaciation on Mars [*Head et al.*, 2005; *Holt et al.*, 2008].

### 2.3. Radar Observations

Orbital sounding radar has been able to extend geologic mapping into the subsurface and has been shown to be effective for both polar ice and volcanic stratigraphy on Mars [*Phillips et al.*, 2008; *Carter et al.*, 2009; *Putzig et al.*, 2009; *Holt et al.*, 2010; *Morgan et al.*, 2013]. In Planum Boreum, the data provide a clear contrast between the lithic-rich BU and the overlying nearly pure water-ice NPLD (Figure 3). Both SHARAD and the Mars Advanced Radar for Subsurface and Ionospheric Sounding (MARSIS) on Mars Express have successfully mapped the regional BU topography with varying degrees of coverage and precision [*Putzig et al.*, 2009; *Selvans et al.*, 2010]. These prior studies provide both a foundation for, and a comparison to, the work we report here.

An early SHARAD study [*Putzig et al.*, 2009] confirmed the first-order BU distribution and morphology as derived from optical methods [*Fishbaugh and Head*, 2005] and gave a first glimpse at the three-dimensional

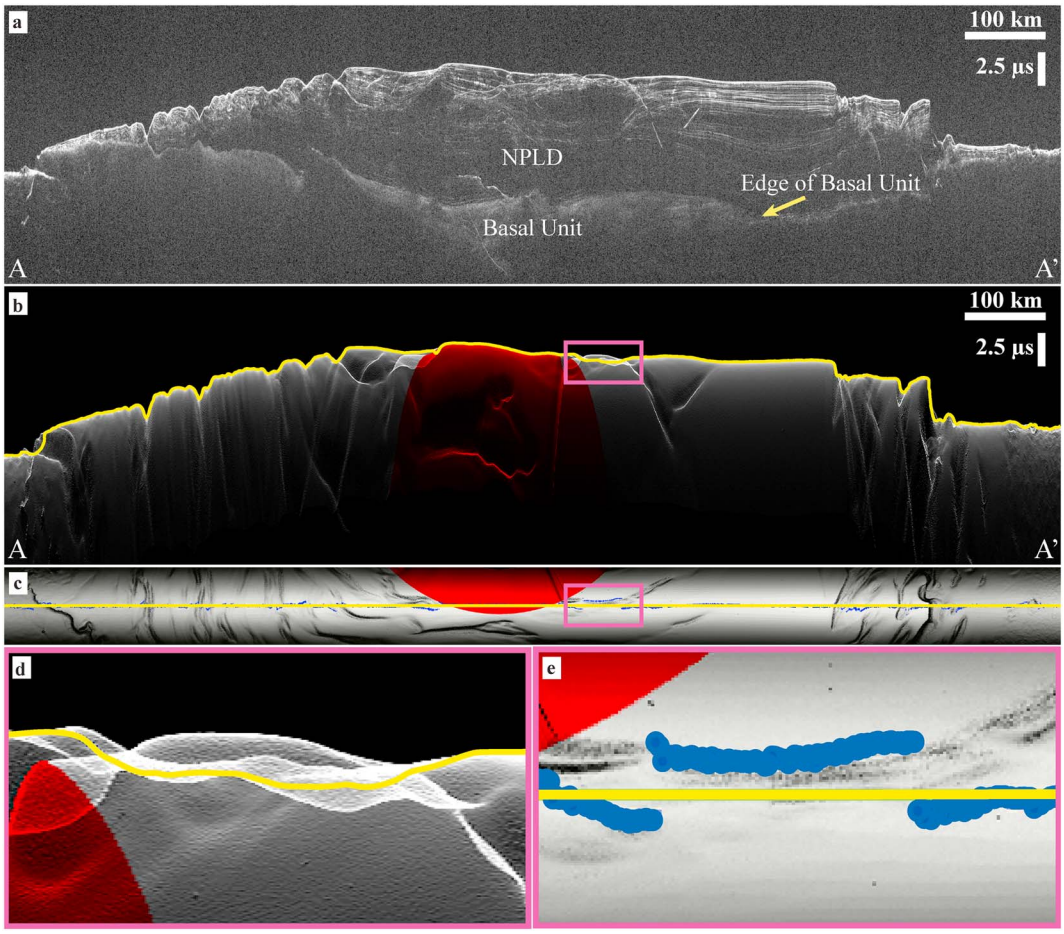


**Figure 3.** SHARAD radar observation 804402000. Location is shown on Figure 1. The vertical scale is one-way travel time. (a) Focused processor Bruce SHARAD radar data shown in time delay. BU return changes from diffuse to sharp near Rupes Tenuis scarp. This radargram also highlights the smooth transition from BU to Vastitas Borealis marked "edge of basal unit." (b) University of Texas clutter simulation. The yellow line on the simulation marks the time delay of the nadir location. Note the edges of Planum Boreum where interpretation becomes more difficult as clutter increases. The pink box shows the location of Figure 3d. (c) Echo power map for the radar return. The blue dots give the first return location, while the yellow line is nadir. The pink box shows the location of Figure 3e. (d) Expanded view of clutter simulation. This section has a large difference between nadir and first radar return. (e) Expanded view of the echo power map covering the same region as in Figure 3d. Note the trough and resulting offset between nadir and first return locations.

structure of the deposit. A later study used MARSIS data to map the BU and estimate its volume [*Selvans et al.*, 2010]. The vertical resolution of MARSIS is approximately 100 m in water ice, an order of magnitude larger than the vertical resolution of 8.4 m for SHARAD [*Picardi et al.*, 2004; *Seu et al.*, 2007]. However, unlike SHARAD, MARSIS excels at penetrating to the base of Planum Boreum allowing it to map the contact between the BU and the underlying Vastitas Borealis Formation for most of Planum Boreum. While the resolution of MARSIS data was lower than the SHARAD study, the work by *Selvans et al.* [2010] confirmed speculations about the BU. Namely, the material composing Olympia Undae appears consistent with the BU mapped beneath Planum Boreum [*Selvans et al.*, 2010]. In addition, MARSIS data gave the first volumetric constraints for the BU using radar data [*Selvans et al.*, 2010]. Both of these radar studies found that the BU contains enigmatic features that cannot be easily explained, including the location of its maximum thickness offset from the north pole and specific locales that radar does not easily penetrate regardless of frequency.

Our study focuses on BU morphology from radar in a similar manner; however, the high resolution of SHARAD combined with dense BU radar mapping reveals additional features that may provide important insights into the early evolution of Planum Boreum. As SHARAD does not consistently sound to the base of Vastitas Borealis, we offer no additional radar-derived constraints for BU composition and instead focus on detailed

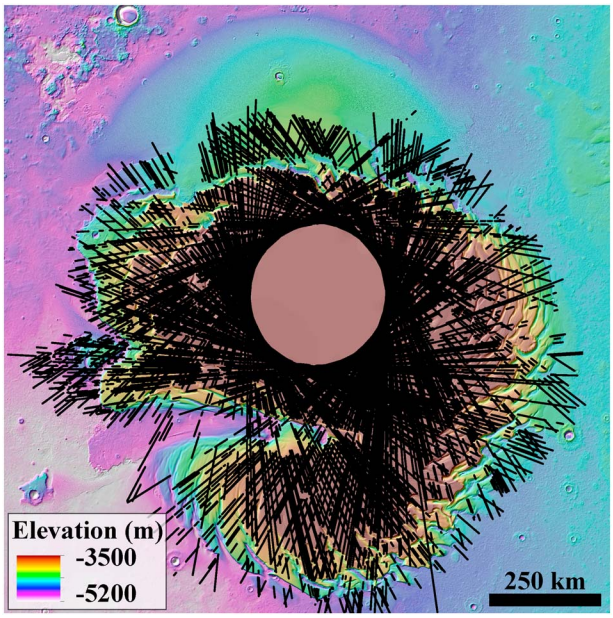


**Figure 4.** SHARAD mapping coverage used to generate gridded data products is shown as black dots. The SHARAD data are on top of colorized MOLA elevation data.

morphologic analysis. Our assumptions pertaining to composition are derived from the optical work presented in section 2.1.

## 3. Data and Methods

### 3.1. SHARAD Data, Processing, and Corrections

SHARAD on Mars Reconnaissance Orbiter (MRO) acquired the primary data used for this study. SHARAD is a radar sounder with a 10 MHz bandwidth and a 20 MHz center frequency [*Seu et al.*, 2007]. Mars Reconnaissance Orbiter has a polar, nearly circular orbit with an altitude of approximately 300 km [*Zurek and Smrekar*, 2007]. This, combined with focused processing, results in a signal footprint measuring ~3–6 km cross track and ~0.3–1 km along track. The bandwidth of SHARAD provides a 15 m free-space resolution and a theoretical vertical resolution of ~8.4 m in water ice [*Seu et al.*, 2007].

Two different processors were used for SHARAD analysis and interpretation. One of the processors ("FPB") makes use of an autofocus routine for correction of ionosphere delays [*Campbell et al.*, 2011]. This processor permits user-defined change of individual parameters such as aperture length, focusing Doppler bandwidth, weighting methods, and ionosphere correction. For mapping of BU deposits, it was qualitatively determined that a long aperture and large bandwidth gave optimal resolution; thus, the FPB product used here has a 6400 length aperture and 0.6 MHz Doppler bandwidth. Comparatively, the additional processors used herein, "FPA" and its successor "QDA," employ a shorter aperture and smaller bandwidth. Radar data presented in this work are labeled to indicate which processor they were derived from. A total of 652 radar observations, or orbital crossings of Planum Boreum, were used to generate the mapping results shown in this paper. Those 652 radargrams provide a total of ~645,000 points that span Planum Boreum and provide high-density coverage of the BU (Figure 4).

### 3.2. Interpretation of SHARAD Data

Radar-based mapping was performed in commercial seismic interpretation environments, both Landmark's DecisionSpace and Schlumberger's GeoFrame. For interpretation, the processed data were converted from binary files into industry-standard SEG-Y files that were then loaded into seismic interpretation environments, map projected, and analyzed. Interpretation of the radar data used reproducible picking algorithms. Both software packages use manually selected reflector locations to locate amplitude peaks present within a customizable time window; this methodology produces consistent results across radargrams and between interpreters. In displayed radargrams the brightness of a reflector is proportional to its amplitude.

Off-nadir echoes, or "surface clutter," challenge orbital radar sounding interpretations. Radar returns from surface features tens of kilometers from the orbit track are often visible in radargrams. While this problem is not as prevalent on the smooth areas of Planum Boreum as in areas with greater topographic relief, it can nevertheless confuse interpretations, especially near steep scarps and polar troughs. A clutter simulation algorithm was developed at the University of Texas Institute for Geophysics that generates synthetic radargrams based on surface topography and MRO orbital geometry [*Holt et al.*, 2008]. This simulation generates a "cluttergram" that predicts the location of all possible surface echoes (rather than attempting to reproduce the radar data) and is used in combination with the radargram to ascertain which signals are from the surface and which are from the subsurface (Figure 3b).

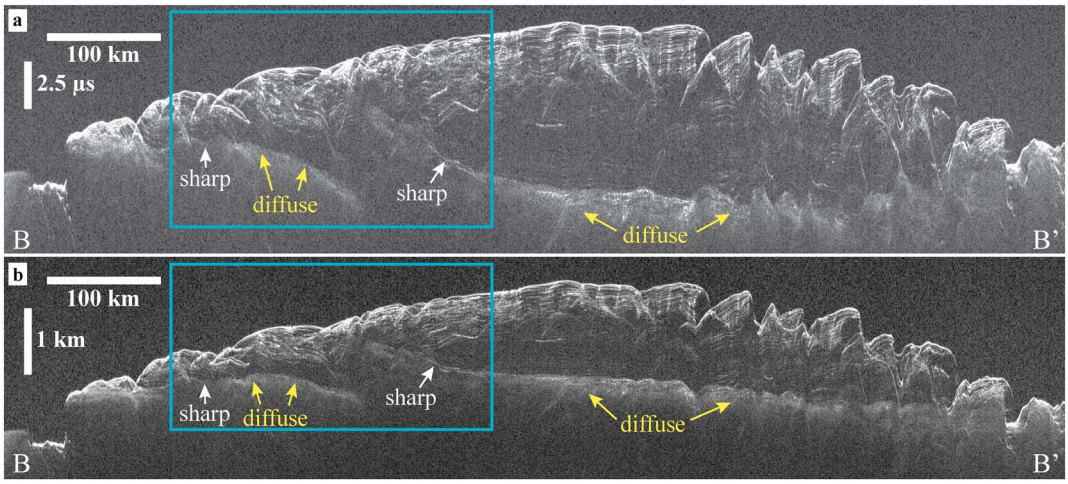


**Figure 5.** Radar observation 521402000. Location is given by the red line in Figure 1. This radargram crosses the BU high and shows the transition from a diffuse BU return to a sharp return. These data are products of the QDA processor, and time is given in one-way travel. (a) Time-delay radar data. (b) Depth-corrected radar data using the real permittivity of water ice ($\varepsilon_r = 3.15$). The blue boxes show the data coverage in Figure 10.

A particular difficulty when mapping a reflector across large regions in two-dimensional data is ensuring that the same reflector is consistently picked. In order to accomplish this, line ties and crossing radargrams were crucial for accurate mapping. Line ties exist where two radargrams intersect. The exact point of intersection is used to continuously interpret two different radargrams as a single observation. In theory, if the radar is penetrating the same location, the subsurface data at that point should be identical between the two radargrams. With crossing SHARAD observations, it is possible to stitch together radargrams creating a complete image that is no longer bound by the path of a single satellite orbit [*Christian et al.*, 2013, their Figure 4]. It is the tying together of different radargrams that enables accurate and robust subsurface mapping. With this technique, complex features can be analyzed from multiple viewing geometries to verify their existence and perhaps uncover their origin.

While specific radar reflectors within the NPLD are difficult to correlate with layers visible in outcrop [*Christian et al.*, 2013], the BU's distinct characteristics offer a unique correlation between radar and imagery. In radar, the transition from NPLD to the BU is generally marked by a change from sharp, well-defined and laterally continuous reflectors to a diffuse zone of radar scattering with few to no internal reflectors. Where this is true, BU is easily differentiable from overlying NPLD. However, in some places the transition to BU is a sharp reflector, similar to overlying NPLD reflectors. In these cases the NPLD/BU transition is assumed to be the lowermost continuous reflector observed. Even though the signature of the BU can change from diffuse to sharp, correlation across and within radargrams supports our BU interpretation of this lowermost reflector (Figure 5).

### 3.3. Data Gridding

Reflector interpretations or "picks" are exported from seismic software packages in ASCII format as along-track sample with time delay and then processed by a series of scripts that convert the reflector time delays into aeroidal elevation with latitude and longitude. This requires registration of the associated surface echo (interpreted in the same manner as the subsurface reflectors) to a known surface elevation. We use the Mars Orbiter Laser Altimeter (MOLA) gridded surface for this [*Smith et al.*, 2001].

The final conversion step provides two exported data products for gridding, each with a different assumption about the location of the first and subsequent echoes [as in *Christian et al.*, 2013]. The *nadir* product positions all of the radar reflectors directly beneath the spacecraft. In contrast, the *first return* product uses MOLA topography and a model of the radar beam pattern to calculate the likely origin of the first signal returned to SHARAD, a location that often, but does not always, coincide with the maximum amplitude return. Individual points are then corrected to this "first return" location, and all subsurface data assume a vertical signal propagation path from the first return location (Figures 3c and 3e). A comparison of gridded data products is shown herein (Figure 6).

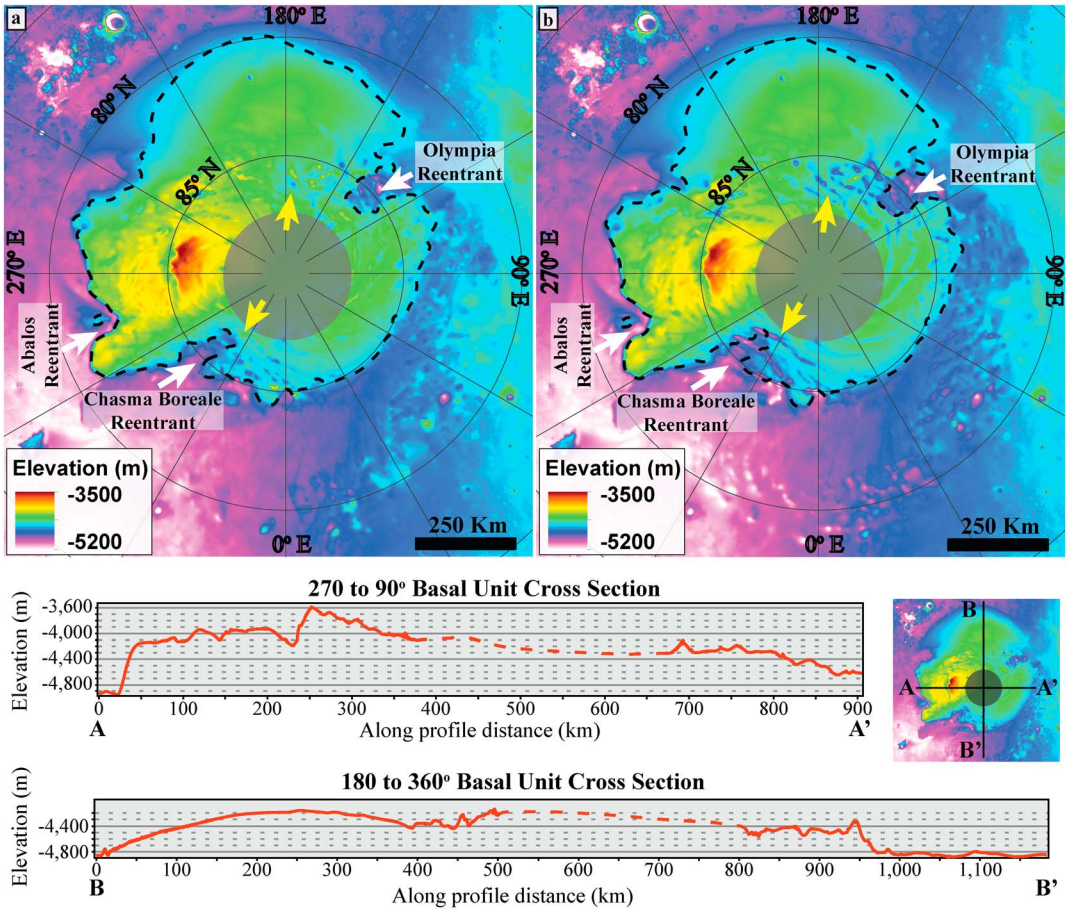


**Figure 6.** Colorized BU top elevation results derived from gridded SHARAD data. Two different data positioning algorithms are shown. (a) Data corrected using the first return technique as discussed in text (preferred version). (b) Data left at nadir location and not corrected. Notice the troughs in the nadir data. These are the result of depth correction without moving the radar data. The yellow arrows point to regions with significant difference between first return and nadir mapping results. In both figures a black dashed line represents the radar-derived extent for BU material. (bottom) Two BU cross sections generated from the first return product. These cross sections highlight the asymmetry of the BU deposit.

Neither approach is perfect for mapping BU structure, as each has strengths and weaknesses. For example, the nadir approach creates artificial peaks in the data directly beneath spiral troughs while the first return approach generates artificial troughs at this same location (Figure 6). From the stratigraphic mapping of trough structures throughout hundreds of radargrams [*Smith and Holt*, 2010, 2015], we know that most troughs originate within the NPLD, not at the BU/NPLD transition. Additionally, trough mapping revealed that these structures migrate poleward. Thus, the surface expression of a trough is typically greater than 30 km northward of where the trough originated, not directly above [*Smith and Holt*, 2010]. Preliminary testing of the first return approach and its use in gridding NPLD stratigraphy indicated it to be nearly perfect for reflectors in the top few hundred meters [*Christian et al.*, 2013]. However, the accuracy of the method appears to degrade with depth, which may be due to a signal propagation path that is more complex than either assumption alone. Both methods assume that the radar data travel vertically downward below the point of surface penetration, and this assumption is likely to produce small errors. The errors generated from the nadir assumption in the BU topography are more pronounced (Figure 6). Therefore, it is our preference to use the first return assumption for positioning radar data acquired over Planum Boreum.

After data extraction and positioning, the interpreted data were gridded. Gridding was performed using Environmental Systems Research Institute (ESRI)'s ArcGIS (Geographic Information System) software. The ASCII files containing reflector interpretations were loaded directly into the program, converted into an

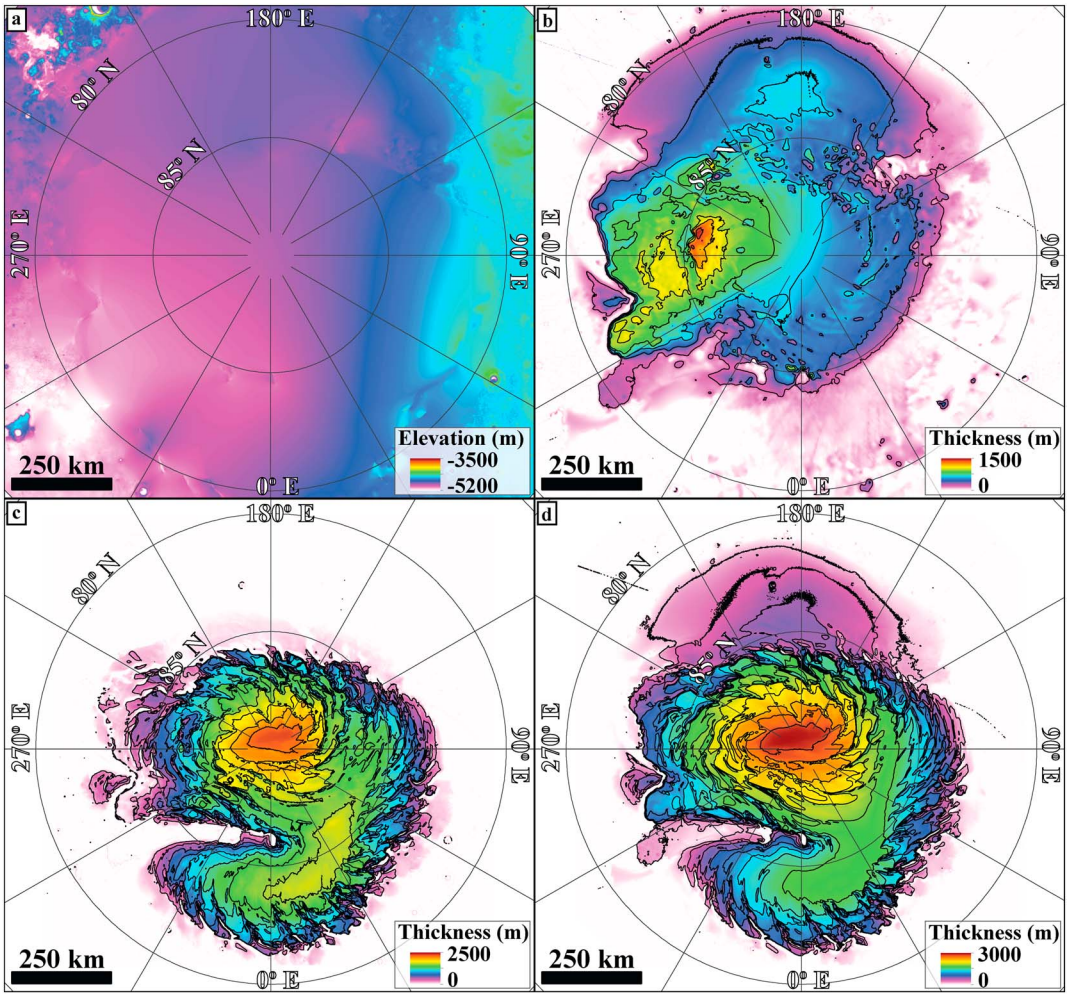


**Figure 7.** Isopach maps for BU and NPLD material. Contours are at 200 m intervals. (a) Topography of Vastitas Borealis after removal of all overlying material including both BU and NPLD. This grid was generated by combination of SHARAD and MOLA shot point data and is used as the base of our subsequent thickness maps. (b) BU isopach map. The Vastitas Borealis grid was subtracted from the first return BU grid to create this product. Note that the maximum thickness is approximately 1500 m. (c) Thickness map of NPLD material. (d) Isopach map for the entire deposit, all material above the generated Vastitas Borealis grid (Figure 7a) is included in these thickness values.

ESRI-compatible format, and interpolated using a natural neighbor algorithm. This method interpolates using weights, similar to an inverse distance weighted approach, but different in that distances used for the weighted mean are calculated from the overlap of Voronoi polygons instead of from a source point [*Sibson*, 1981]. A resolution of 256 pixels per degree was assigned for the output raster products. SHARAD does not acquire data north of 87.5° latitude due to its polar orbit; however, we do interpolate across the polar data gap. Our mapping products cover this data gap with a dark oval to emphasize the uncertainty of SHARAD gridding north of 87.5°.

Gridded data were used for analysis of the BU and for all volumetric calculations pertaining to BU and overlying NPLD. For the purposes of volumetric BU calculations, the Vastitas Borealis base was assumed smooth, created by the interpolation of a small number of MOLA shot point data in conjunction with SHARAD interpretations of the Vastitas Borealis surface where BU is either not present or relatively thin (Figure 7). In general, SHARAD seldom penetrates to the interface of Vastitas Borealis Formation and BU. Therefore, this study does not attempt to define a dielectric constant for BU material. We rely on MOLA values, SHARAD where BU is either not present or relatively thin beneath the NPLD, and interpolation to define the Vastitas Borealis base.

### 3.4. Reentrant Volume Estimations

To estimate the volume of eroded BU material we first created the BU topography without any reentrant morphology. This surface is the hypothesized prereentrant configuration of basal unit material. To accomplish this, interpolation was done across each reentrant using only boundary elevation values. This methodology assumes that deposition was initially continuous and uniform across the area now containing a reentrant. From the newly created surface, we subtracted the elevation of the modern BU topography generating a thickness raster for eroded material. Within ESRI's ArcGIS we were able to use these constructed isopach maps to calculate the hypothesized missing BU volume from each reentrant. These estimates do not include the widespread erosion of BU material not directly associated with each reentrant.

Calculation of the surrounding terrains' dune volume was done using a similar methodology. Equivalently, we interpolated across the landforms of interest using boundary elevation values. However, unlike the reentrants, this generated an underlying surface instead of an overlying surface. Once again, subtracting the lower surface from the upper surface gave us isopach maps, which were then used for volumetric calculation and comparison.

### 3.5. Mesoscale Wind Modeling

The BU topography, distinct from the overlying modern NPLD topography, was used to conduct a preliminary regional climate simulation over the north pole of Mars. This preliminary regional climate simulation was done using the Laboratoire de Météorologie Dynamique (LMD) Martian mesoscale model [*Spiga and Forget*, 2009]. While our initial gridded topography was created at 256 pixels per degree (ppd) resolution, topography used by the model was down sampled to 64 ppd (~920 m resolution) using the nearest neighbor algorithm to derive cell values. At its outer boundaries, the 64 ppd BU topography was merged with 64 ppd gridded MOLA topography generating a complete northern hemisphere of Mars for input into the LMD mesoscale model [*Spiga and Forget*, 2009]. To account for the polar data gap north of 87.5° latitude, we interpolated across this void using values consistent with those at the boundary. We then generated wind maps at 6 km resolution for Planum Boreum over a complete diurnal cycle. The modeling is intended to be illustrative rather than conclusive: compared to present-day regional climate simulations of Mars' north pole, the only difference is topography. Clearly, other changes in climate properties (such as obliquity and dust opacity, see *Forget et al.* [2006] and *Madeleine et al.* [2009]) should be taken into account to carry out a complete quantitative modeling study.

## 4. Results

This study has produced the most detailed subsurface map of BU topography yet available (Figure 6). The results here are significantly different from early Planum Boreum BU maps [*Byrne and Murray*, 2002; *Tanaka et al.*, 2008; *Selvans et al.*, 2010] and improved from the previous SHARAD study [*Putzig et al.*, 2009] with greatly increased mapping density and coverage. An important consideration is that due to the orbital inclination of MRO, no radar data exist north of 87.5° latitude; therefore, our gridded maps have been masked north of that latitude.

Our results for BU extent show a highly asymmetric, ~700 km wide deposit (Figure 6). The thickest mapped portion of this deposit is located at 85.7°N and 265°E, offset from the center of Planum Boreum. There, the BU has a thickness much greater than 1 km, assuming a smooth base for Vastitas Borealis (Figure 7).

There is a geographic pattern to the differing BU radar return properties discussed in section 3.2. Near the BU topographic high, the return is sharp and bright (Figure 3). This indicates a strong dielectric contrast with a relatively smooth surface, resulting in low scattering losses. However, near the periphery of the BU at the east, the NPLD-BU transition is a diffuse radar interface. This style of return is hypothesized to result from scattering of the radar signal and is easily distinguished from sharp radar reflections. A more detailed analysis of the significance of this dualistic BU radar reflection character will be addressed in the discussion section.

With the BU high as our point of reference, the eastern and western hemispheres (in polar projection) express markedly different morphologies. In terms of longitude, this referencing corresponds to a separation of 0° to 180° as the eastern half and 180° to 360° as the western half. The east half is characterized by a low, smooth slope that makes a gradual and continuous transition from the BU high onto Vastitas Borealis. The west has a

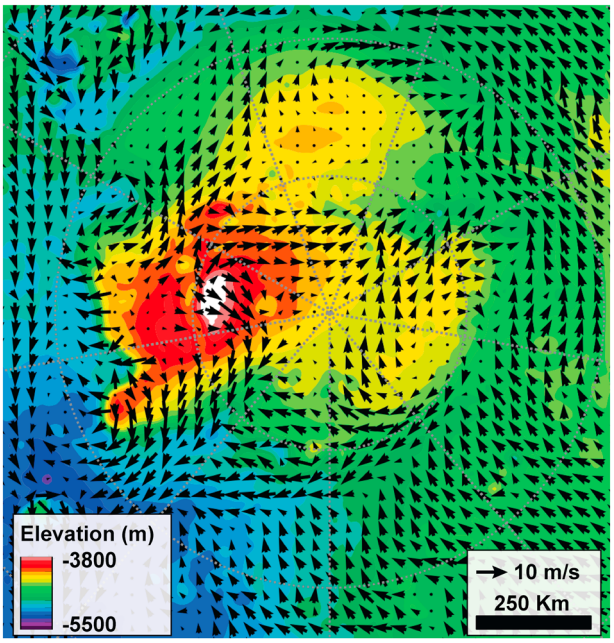


**Figure 8.** Mesoscale wind modeling results using SHARAD paleotopography. Topography is color shaded by elevation, and vectors show the wind magnitude and direction. The modeled winds for Planum Boreum are largely consistent with time. Shown here is a midday time step.

steep slope following the BU high, a trough, and then a flat, broad deposit (Figure 6). At the edge of the western BU is the Rupes Tenuis scarp, where the BU is abruptly truncated.

Three features resembling reentrants are evident in the BU (Figure 6). Two of these features are found in the vicinity of, but not coincident with, present-day Chasma Boreale, while the third is found near present-day Olympia Cavi. These reentrants are variable in size ranging from 50 km to over 100 km long. In addition, the general morphology of these features is variable with no obvious correlation.

Predicted winds generated via mesoscale modeling using BU topography (Figure 8) show strong topographic control, with flow away from the BU summit. The winds move outward with Coriolis deflection, similar to the modern wind flow [*Howard*, 2000] and modern modeling results [*Spiga et al.*, 2011], an expected result given our simple illustrative modeling where only the topography is modified when compared to present-day conditions. The weakest winds are south of the BU high trough, directly over Olympia Undae, and over the north pole data gap where topography was smoothly interpolated across (Figure 8). In addition, weak winds are located at the periphery of Planum Boreum following their sharp acceleration over the deposits edge. Consistent winds are found south of Planum Boreum, with a nearly constant 4–5 m/s wind velocity, in stark contrast to central Planum Boreum's frequently changing wind vectors (Figure 8).

## 5. Discussion

### 5.1. BU Extent

In the west, the only surface exposures of the BU margin are along the Rupes Tenuis scarp and within Chasma Boreale. The Rupes Tenuis scarp creates the edge of the modern BU extent in the Abalos region (see Figure 1). Elsewhere, BU is covered by NPLD, preventing direct optical-based determinations of the BU margin location [*Byrne and Murray*, 2002; *Herkenhoff et al.*, 2007; *Tanaka et al.*, 2008; *Warner and Farmer*, 2008b; *Kneissl et al.*, 2011]. *Tanaka et al.* [2008] hypothesize a vertical kilometer of BU erosion at Rupes Tenuis, the location of rupes unit exposure. Kilometer-scale erosion in combination with crater counting supports hypothesis that the BU is significantly older than the overlying NPLD [*Tanaka et al.*, 2008]. However, optical mapping could not verify the buried extent of the BU's truncated edge. Subsurface stratigraphy revealed by the SHARAD data set and mapped in this study allows us to expand upon these initial observations of BU extent and morphology. In addition, we compare the results of our study to the earlier SHARAD study [*Putzig et al.*, 2009] to ascertain the impact of increased data coverage on mapping results.

While the BU boundary from approximately 240°E to 300°E exhibits a steep scarp and widespread erosion, this study reaffirms that the erosional character of the Rupes Tenuis scarp is a localized feature. Elsewhere beneath Planum Boreum the BU transition to Vastitas Borealis is a smooth transition (see Figure 3). Note that a smooth transition does not mean that the BU on the eastern edge is without erosion; it only indicates that erosion on the eastern edge, if present, was a different process and did not result in the same morphology as that on the western edge. Impact craters and associated, armored surfaces have been observed on the western side and may be responsible for the distinct erosional properties there. Impact ejecta armoring

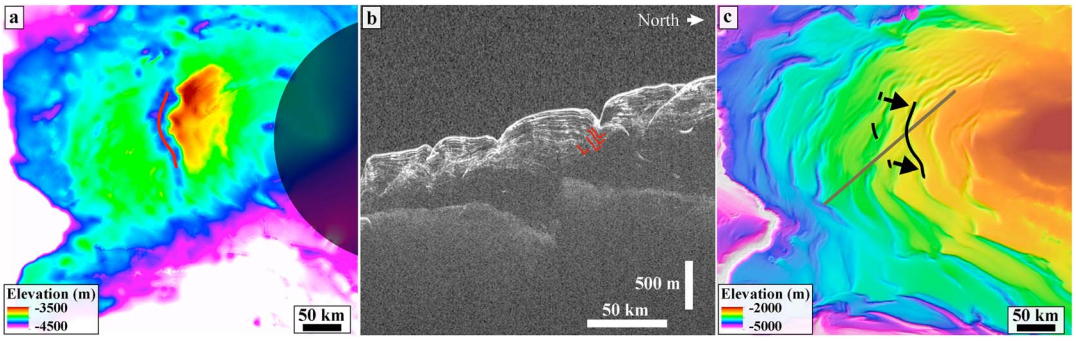


**Figure 9.** (a) Expanded view of the BU color-shaded topography centered on the depression near the high. A red line is drawn on this feature for comparison with Figure 9c. (b) Depth-corrected radar observation 1088302000. The reflectors traced in red highlight a tentative trough migration path that may result from the BU trough. Location is shown by the grey line in Figure 9c. (c) MOLA topography over the BU high. The dashed black line gives the position of the BU depression. The arrows are drawn from the BU depression to a modern trough with similar morphology.

may have resisted erosion [*Arvidson et al.*, 1976], creating the large relief of Rupes Tenuis [*Tanaka et al.*, 2008], whereas the eastern half was not armored, and therefore eroded with a smooth transition to Vastitas Borealis. The remaining margins, toward Olympia Undae and Gemina Lingula, exhibit smooth edges and transitions to the Vastitas Borealis Formation, with only minor irregularities in specific regions. As presented by *Selvans et al.* [2010], we also find that the BU is smoothly contiguous with Olympia Undae and that the dune field there is likely composed of, and underlain by, BU material. Thus, the Olympia Undae dune field is included in our work as part of the modern BU extent.

### 5.2. Depocenters

In previously published radar studies, BU mapping indicated that the thickest BU deposit is offset from 90° latitude [*Putzig et al.*, 2009; *Selvans et al.*, 2010]. As the thickest portion of Planum Boreum is very near 90° (Figure 7), if the BU and overlying NPLD were formed from similar processes in a similar climatic and orbital configuration, one would expect the thickest BU deposit to also be near 90°. Our work establishes that the offset is to the south along the 265°E meridian, with the BU maximum thickness located at approximately 85.7°N, 265°E (Figure 7). This result is similar to the previous SHARAD study [*Putzig et al.*, 2009] but significantly different from MARSIS results [*Selvans et al.*, 2010].

We hypothesize that the mapped BU maximum thickness corresponds to the location of the BU's depocenter. This assumption is supported by the presence of isolated rupes unit material south of Planum Boreum between 240° and 330° longitude [*Tanaka and Fortezzo*, 2012], the steep nearby Rupes Tenuis scarp which directly contrasts the transition from BU to Vastitas Borealis Formation mapped from 0° to 180° longitude, and the lack of evidence supporting increased deposition within the polar data gap. The BU radar return along the edge of the data gap continues trending downhill. In fact, the SHARAD data contain no evidence that the basal unit elevation increases north of 87.5° latitude. The BU maximum thickness' proximity to the Rupes Tenuis scarp both supports the claim that this area is the depocenter and reinforces the need for large-scale BU erosion along the scarp. Without erosion, the basal unit should have extended much farther past Rupes Tenuis than it does currently, assuming coarsely symmetrical deposition. The hypothesized offset center found in SHARAD mapping agrees with observed erosion of BU from Rupes Tenuis, the mapped BU outlier material, and the nearly flat-lying bedding in Rupes Tenuis [*Tanaka et al.*, 2008; *Warner and Farmer*, 2008a; *Kneissl et al.*, 2011; *Tanaka and Fortezzo*, 2012]. Furthermore, if the depocenter was not located at the BU high but instead nearer to 90°, additional impact armoring and a more complicated scenario would be required to create our mapped morphology given the observed aeolian erosional processes.

While the location of the thickest BU mapped in this work agrees with that of *Putzig et al.* [2009], other features associated with the high point are revealed in our study; in particular, a linear depression south of the BU high is apparent that mimics the morphology of a nearby modern trough (Figure 9). Although most polar troughs originated within the NPLD [*Smith and Holt*, 2015], it appears possible that at least in this location, the morphology of a trough-like feature in the BU may have propagated into the NPLD and

**Table 1.** Volumetric Results of This Study Compared With Previous Results[a]

| Feature | Calculated Volume—This Study ($10^6$ km$^3$) | Previous Volumetric Results ($10^6$ km$^3$) |
|---|---|---|
| Basal unit | 0.38 (SHARAD) | 0.45 (MARSIS) |
| NPLD | 0.79 (SHARAD) | 0.78 (MARSIS) |
| Planum Boreum | 1.17 (SHARAD) | 1.3 (MARSIS), 1.14 (MOLA) |
| Abalos reentrant | 0.003383 (SHARAD) | |
| Abalos dune field | 0.000523 (MOLA) | |
| Reentrant within Chasma Boreale | 0.003654 (SHARAD) | |
| Hyperborea Lingula | 0.003316 (MOLA) | |

[a]Reentrant and related feature calculations were performed via interpolation as described in section 3.4. Previous volumetric results are from *Selvans et al.* [2010] for MARSIS data and *Smith et al.* [2001] for the MOLA comparison. The volume calculated for Planum Boreum is very similar for MOLA and SHARAD results.

migrated northward similar to other trough migration patterns [*Smith and Holt*, 2015]. However, SHARAD data have shown no conclusive link between the linear depression and overlying spiral troughs. Reflectors directly above the BU trough are virtually nonexistent in SHARAD data, and trough migration path tracing here requires large assumptions about migration path.

Using our BU mapping results and our interpolated Vastitas Borealis surface we generated isopach maps for NPLD and BU material (Figure 7). We calculate and include in Table 1 the volume of BU, NPLD, and Planum Boreum. In Table 1 we also include previously published results derived from MARSIS [*Selvans et al.*, 2010] and MOLA [*Smith et al.*, 2001] for comparison. These volumes will help provide constraints for Martian water budget estimations. The MARSIS-based radar study of *Selvans et al.* [2010] indicated that the thickest region of NPLD deposition was at 30°E longitude and ~1800 m in thickness. Both the location and thickness in our study differ significantly. Our study finds the maximum NPLD thickness to be ~2350 m and located at 105°E longitude and 87.5° latitude; however, it is likely that there is additional thickness north of 87.5° based on trends in our isopach maps with respect to the gap in data coverage above 87.5° latitude. It is important to note that the theoretical resolution of SHARAD and MARSIS differ by an order of magnitude. In practice, the two instruments have even greater difference due to the ionospheric interference suffered by MARSIS with its lower operating frequency, and it is therefore our preference to rely on SHARAD results.

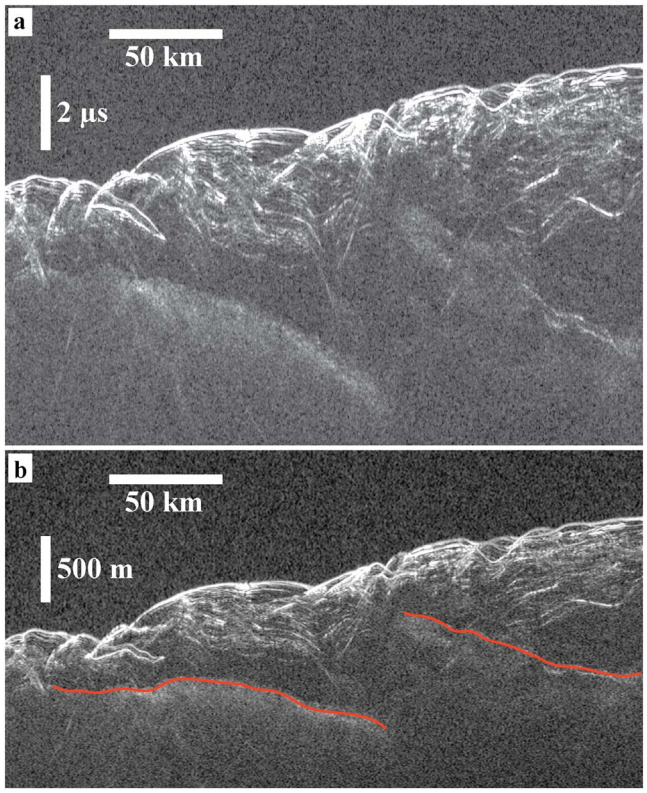


**Figure 10.** Radargram 521402000 enlarged to show BU truncation on the west side of the high. See Figure 5 for context. (a) One-way time and (b) depth corrected using a real permittivity of 3.15. The red line denotes the interpreted transition from NPLD to BU material.

The difference in locations for BU and NPLD maximum thicknesses emphasizes that different patterns of accumulation likely dominated each deposit. We posit that the shift of depocenter from the 240° longitude line for the BU toward the pole for the NPLD is the result of atmospheric influences, although determination of a specific cause is beyond the scope of this work.

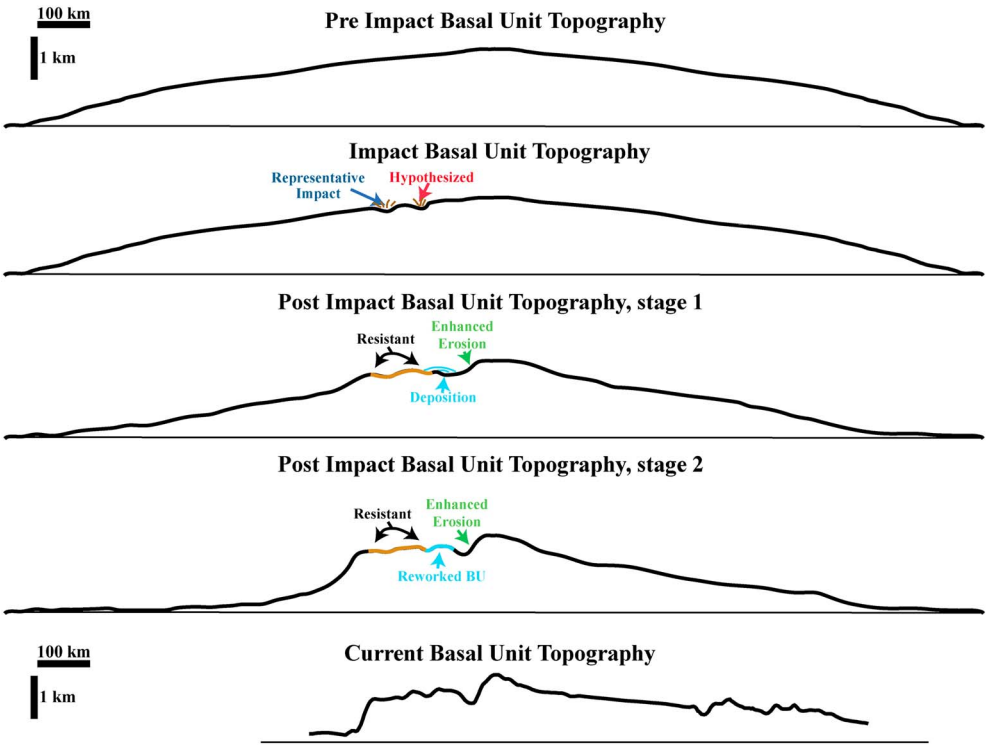


**Figure 11.** Hypothesized evolution of the BU topography. Transect is coincident with radar observation 521402000, and the location is shown in Figure 1 (red line). Representative impact events along Rupes Tenuis are labeled along with the location of our hypothesized impact. The impacts result in ejecta armoring and a resistant layer. Katabatic winds and differential erosion, resulting from the impact armoring, dictate landform evolution in the postimpact BU figures.

### 5.3. BU Morphological Irregularities: Hypothesis and Implications for Cavi Unit

The BU high is immediately poleward of a prominent, arcuate depression. In contrast to the nearly uniform 0.1°–0.4° slopes found elsewhere on the BU surface, the depression is defined by an equator-facing slope that varies from ~2.5° to 4.0°. This value is comparable to the ~3° slopes of modern spiral troughs prevalent in this region [*Smith et al.*, 2013; *Smith and Holt*, 2015]. In radargrams the depression appears to truncate the BU (Figure 10), suggesting that it is erosional in nature. Any explanation for the BU morphology in this region must describe the genesis of the BU high, the steep slope defining its equatorward edge, the trough found at its base, and the relatively thick, flat, BU surface extending between the trough and the modern margin of the unit. Here our use of the word trough is intended only to describe the quasi-linear topographic low directly equatorward of the BU high and is not intended to imply that this BU feature is equivalent in origin to the modern spiral troughs (although it could have initiated subsequent trough formation in the NPLD).

Our explanation for the BU high, as discussed in section 5.2, assumes that it was originally the center of rupes deposition, that asymmetric aeolian erosion resulting from material differences led to the differences between eastern and western regions. This hypothesis takes into account the aeolian origin of the basal unit [*Tanaka et al.*, 2008], offering explanation for both genesis and location of cavi material. We suggest the BU high has always been the thickest part of the deposit. Observations of BU outcrops around Planum Boreum have noted the presence of impact-related deposits on the western exposures but not the eastern [*Tanaka et al.*, 2008]. An approximately 100 km poleward extension of these impact events in the western half of the deposit would have resulted in the formation of additional armored ejecta, which can retard erosion [*Arvidson et al.*, 1976]. We additionally posit that no armoring was present on the BU high. The rupes unit, in particular, is known to have undergone extensive erosion with ~1 vertical km or more of material removed along Rupes Tenuis [*Tanaka et al.*, 2008].

The large extent of rupes erosion becomes important when considering the potential role of armored deposits in influencing BU morphology. Erosion of the unarmored BU surface adjacent to armored deposits would have

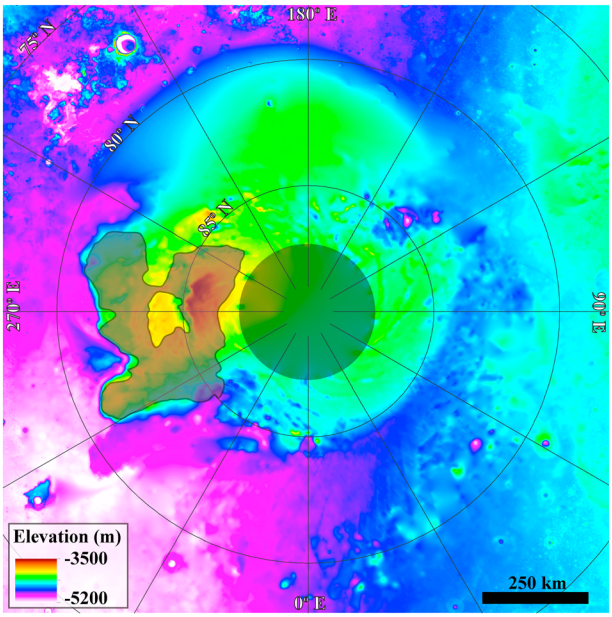


**Figure 12.** The extent of sharp SHARAD BU radar returns is shown by the semitransparent black polygon overlapping colorized BU topography. Our work hypothesizes that the sharp radar return is from rupes unit without cavi. The lack of a sharp return downwind of the BU topographic high is likely the result of deposited, reworked, rupes material downwind of erosion.

been irregular. Furthermore, asymmetry in the distribution of impact deposits would have led to deposit-wide asymmetric erosional patterns as has been observed for the south polar layered deposits [*Kolb and Tanaka*, 2006].

Both local and regional characteristics, including the trough and the drastically different morphologies of the western and eastern halves of the BU surface, can be explained by our hypothesis (illustrated in Figure 11). A simplistic mounded deposit was used as a starting point for our hypothesis, and we acknowledge the low probability of a smooth symmetrical BU predecessor. This simplified surface can be made more complex without significantly altering our proposed erosional scenario, but there is no basis on which to define a specific topography that is more complex. Beginning with a preexisting high, katabatic winds shed off the high to the west would have encountered both armored and unarmored deposits. It is feasible that the trough originated as a zone of easily eroded, unarmored sediment. Topographically enhanced through continued erosion, it continued to evolve into the current feature, characterized by an equator-facing slope of magnitude comparable to modern slopes of the wind and sediment transport-driven spiral troughs. The broad, relatively flat feature between the trough and the deposit margin can be explained as the result of flow deceleration out of the trough and the deposition of eroded sediments in this region. Katabatic winds shed off the high to the east, however, encountered no such irregularities in surface properties that modify erosion. In the absence of armored ejecta deposits, material was eroded and distributed more uniformly, generating asymmetry in the gross morphology of the BU surface (Figures 6, 7, and 11).

Optical and SHARAD-based mapping of the distribution of cavi unit supports the proposed hypothesis. Estimated to be Middle Amazonian in age, the cavi unit represents a transitional member between the BU and overlying NPLD that was deposited during and/or after erosion of the rupes unit [*Tanaka et al.*, 2008]. It is reasonable to assume that the substantial erosion of the rupes unit provided the loose sediment needed to accumulate the cavi. Therefore, the cavi's distribution is intimately related to rupes morphology and the distribution of armored impact ejecta. Mapping in SHARAD data has distinguished two types of returns from the top of the BU: sharp and diffuse. Notably, sharp BU returns exist primarily in the vicinity of the BU high as well as in the western half of the deposit, while diffuse returns dominate the eastern half and the flat area directly equatorward of the trough (Figure 12). The lateral segregation of sharp and diffuse reflectors corresponds with the hypothesized locations of, respectively, wind-scoured rupes and deposition of eroded material as part of the cavi unit. Given the different depositional styles of the rupes and cavi units [*Herkenhoff et al.*, 2007; *Tanaka et al.*, 2008] and resultant implications for radar returns [*Putzig et al.*, 2009], this hypothesis is reasonable. Rupes unit is exposed along the Rupes Tenuis scarp, and it is at this location that the radar return is bright and sharp (Figures 3 and 12). Locales with exposed cavi unit are generally diffuse; however, there are inconsistencies between radargrams, and diffusivity appears to be less of an indication for composition than a sharp radar return. Diffusivity can be the result of ionospheric dispersion of the radar signal, volume scattering from within the material, or off-nadir scattering from a rough interface at the top of the deposit.

Additional support for the subsurface distribution of rupes and cavi resulting from patterns of deposition and erosion is provided by image analysis of Planum Boreum's margins. Notably, the greatest occurrences of cavi

unit, a product of rupes erosion, are in Olympia Cavi [*Tanaka et al.*, 2008], which exists in the eastern half of the BU deposit, and proximal to our mapped diffuse SHARAD BU returns. In these locations the lack of armored deposits and local topographic influence due to the presence of armored deposits, respectively, led to an increase of cavi deposition. This is comparable to the known formation mechanism of the cavi outlier beneath Abalos Mensa, where erosion of the Rupes Tenuis scarp in combination with local wind patterns led to the accumulation of the wedge-shaped mound of sediment [*Brothers et al.*, 2013]. Rupes unit exposures are consistent with locales where the sharp BU return is mapped to the edge of Planum Boreum.

The hypothesis presented here for the distinct morphology of the BU is significantly different from prior hypotheses. Initial investigation of the BU high explained its existence by a single impact event directly over the high point, which subsequently armored the high from erosion, while the unarmored material around it was eroded and transported away [*Putzig et al.*, 2009]. In this hypothesis the modern morphology of the BU results solely from the occurrence of a single impact event. Additionally, this hypothesis should result in symmetrical erosion around the BU high. Given the intricacies of aeolian systems, it seems more likely that the morphology was driven by a combination of initial depositional and later erosional processes. Provided an antecedent topography resulting from regional depositional patterns, katabatic winds from the depositional high in conjunction with asymmetrically distributed armored impact ejecta are able to explain not only the irregular local topographic features of the BU but also its nonuniform surface morphology (Figure 11).

### 5.4. Analysis of the Three Major Reentrants in the BU Deposit

In addition to BU irregularities due to offset of the depocenter from 90° latitude and asymmetric erosion, the unit also contains three prominent reentrants that result in further morphologic irregularity. These cutbacks into the BU deposit are variable in size and morphology. As only three substantial reentrants have been uncovered, it would also appear that they are not representative of typical processes in the BU and required special circumstances to form. Mapped reentrants clearly impact overlying deposition and provide additional information about the nature of ice deposition following BU emplacement.

One major reentrant is in the Abalos region and bounded by the modern Rupes Tenuis scarp (Figures 1 and 9). As SHARAD data for this feature were analyzed in a prior publication [*Brothers et al.*, 2013], it will only be mentioned briefly here. The topography of Abalos has been heavily influenced by this reentrant—everything from dune deposits radiating away from the ice cap to the isolated wedge of cavi unit and NPLD forming Abalos Mensa are the result of the reentrant and the Rupes Tenuis scarp. The dune field along the eastern edge of Abalos Mensa has sand hypothesized to be of BU origin [*Byrne and Murray*, 2002; *Tanaka et al.*, 2008], and all of this sand might have been sourced from the BU reentrant that created Rupes Tenuis. We estimate the volume of material removed from the Abalos reentrant and compare that to the volume of material present in the dune field (Table 1). Dune field volume was obtained using MOLA topography and a base constructed by interpolating between interdune elevation points. The subtraction of the interpolated base from the MOLA top is the volume we use for the dune field. Our results indicate that Abalos basal unit erosion is more than sufficient to supply the local dune field. Only 30% of the eroded material must remain if rupes is 50% sand by volume. The excess sand was likely transported to another portion of the circumpolar erg.

A second reentrant is not readily apparent in Planum Boreum's modern topography. This reentrant is located at ~300°E longitude and extends from the northwestern wall of present-day Chasma Boreale to 87°N (Figure 6 and Figures 13a and 13b). It measures approximately 110 km wide and 150 km long and is larger than the Abalos reentrant. Using the same methodology as with the Abalos reentrant, the volume of BU material removed to create this reentrant was calculated with the results given in Table 1 (assuming that it is entirely erosional). The result of this erosion is likely the formation of either the lobe of material that is Hyperborea Lingula (Figure 1) or dunes within Chasma Boreale, resting on top of Hyperborea Lingula. Unlike in the Abalos region, the dunes that exist in Chasma Boreale are less clearly linked to the reentrant, and we do not analyze them separately with our volumetric analysis. We estimate that nearly all of the BU sediment removed from this reentrant would have needed to remain as Hyperborea Lingula to account for the lobe's volume (Table 1). This result is in a stark contrast to the Abalos reentrant and an unlikely scenario; however, studies have indicated that Hyperborea Lingula may in fact be partially preserved rupes unit [*Tanaka et al.*, 2008] Alternatively, if the reentrant within Chasma Boreale is only responsible for the dunes atop Hyperborea Lingula, then just a small fraction of the sediment is required, which could potentially be sourced directly

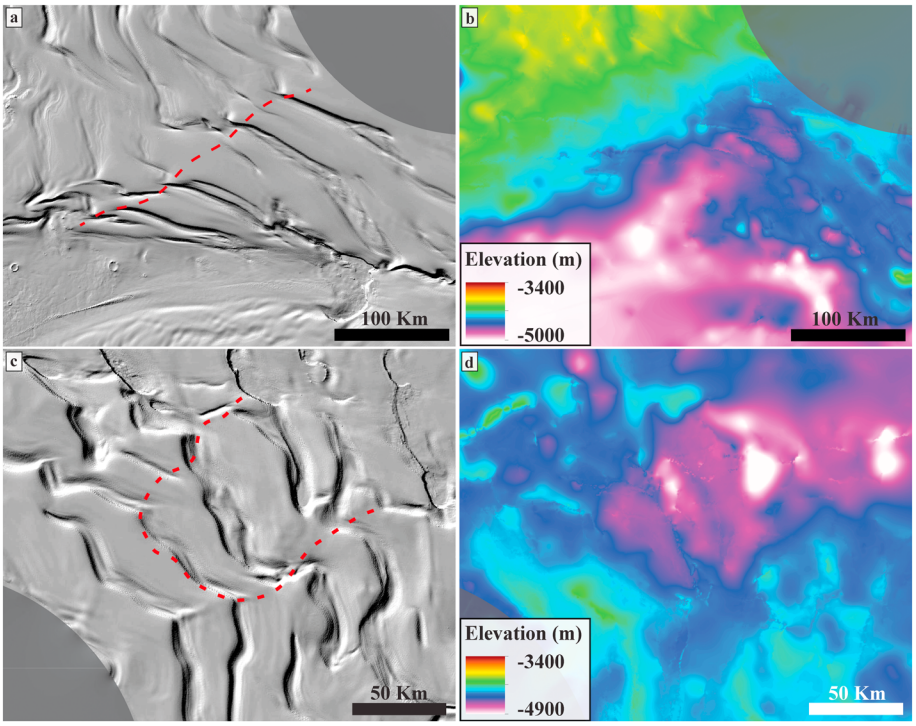


**Figure 13.** (a) Shaded-relief image created from MOLA topography showing the edge of the reentrant adjacent to Chasma Boreale with a dashed red line. Note how this line follows a linear ridge in the modern topography. (b) Colorized BU topography for the reentrant within Chasma Boreale. (c) MOLA-derived, shaded-relief image showing Olympia Cavi reentrant outline in dashed red. The outline of the reentrant is coincident with irregular trough morphology. (d) Colorized BU topography for the Olympia Cavi reentrant. Location for Figures 13a–13c is given in Figure 1.

from erosion of the reentrant. It is also important to note that given sufficient exposure time, eroded BU material may have been removed via saltation and transported into the circumpolar erg [*Tanaka and Hayward*, 2008].

Another interesting morphology associated with the reentrant adjacent to Chasma Boreale is an aligned series of deflections and terminations of spiral troughs forming a roughly linear ridge in the modern NPLD topography above the southern edge of the reentrant. This topographic ridge directly overlays the reentrant boundary (Figures 13a and 13b). While the fate of the removed sandy material is still unresolved, it is evident that the reentrant, and therefore BU topography, likely impacted deposition of the overlying NPLD at this location, creating a linear scarp aligned with the reentrant's border. This is a good example of BU topography impacting modern ice cap features.

A third reentrant is located at ~132°E, 85°N (Figure 6 and Figures 13c and 13d). This reentrant differs from the first two because there is no evidence for an associated circumpolar deposit. There are, however, several cavi unit exposures nearby in the Olympia Cavi region. The presence of cavi unit near a reentrant is consistent with hypothesis that the eroded rupes unit forms the Planum Boreum cavi unit. This reentrant is nearly circular with an opening at the southern edge. While the nearest unconsolidated sedimentary deposit is Olympia Undae, which may or may not have been sourced in part by the creation of this reentrant, this feature does have a visible impact on the overlying NPLD, similar to the reentrant adjacent to Chasma Boreale. At the northern edge of this reentrant, the NPLD exhibits a similar pattern of concentric ridges that follow the reentrant outline (Figure 13c). Prior work based on imagery mapped surface features similar to grabens in this location [*Tanaka et al.*, 2008]. A graben-like surficial signature has not been identified elsewhere on Planum Boreum [*Tanaka et al.*, 2008], yet is found in direct proximity to a BU reentrant. Therefore, it is possible that relief associated with the subsurface BU reentrant at this locale is responsible for the unique NPLD deposition and surface features found here. Of the nine mapped graben features in *Tanaka and Fortezzo* [2012], seven are within the bounds of this reentrant while the remaining two are nearby

to the southwest. BU reentrants appear to alter NPLD deposition, creating features found nowhere else on Planum Boreum. The observed vertical translation of antecedent topography is characteristic of aeolian rather than glacial processes.

### 5.5. Katabatic Wind Modeling With BU Topography

The wind modeling performed in this study was intended to aid the investigation of Planum Boreum cavi unit and earliest NPLD depositional and erosional processes. This modeling does not attempt to reconstruct paleoclimate nor quantitatively describe the winds that modified the cavi unit and NPLD. Additionally, we do not believe that the winds modeled here are representative of winds that deposited rupes unit, as climate conditions for early rupes were likely significantly different from those used in our modeling. For the interpretation of modeling results we assume that cavi and NPLD are a nearly continuous formation, as is supported by their gradational contact [*Tanaka et al.*, 2008]. Therefore, the relevant climate parameters for the cavi unit and NPLD should be very similar and only slightly different from the modern climatic conditions, as used for these simulations. This modeling functions as a qualitative test of our understanding of polar processes, namely, aeolian, given the mapped BU morphology.

Investigation of Planum Boreum's BU has revealed features commonly associated with erosion, such as reentrants and troughs. We have attributed this erosion to wind, as modern observations indicate that wind is actively reworking the NPLD [*Howard*, 2000; *Smith and Holt*, 2015]. Our mesoscale simulations using BU topography show that the resulting winds generally agree with wind circulation obtained over modern topography [*Spiga et al.*, 2011], with notable exceptions. It is important to remember that the BU topography used in this modeling is the result of substantial erosion and has likely evolved with aeolian forces. Important differences between our BU wind maps and modern wind maps are primarily above the BU reentrants.

As discussed by *Brothers et al.* [2013], modeled paleowinds over Abalos where the Abalos Mensa deposit now exists are almost nonexistent, in stark contrast to the modern wind fields that are strongly influenced by the current Abalos Mensa mound. Modern wind fields show katabatic winds flowing down and away from Abalos Mensa [*Spiga et al.*, 2011]. Without the mound's presence the model does not produce these additional katabatic winds. Another difference is along Chasma Boreale. As the chasma had not yet been constructed at the time of BU deposition [*Holt et al.*, 2010], the winds through this region are not deflected down the chasma but are instead deflected through a reentrant within the BU, until they later follow the topographic break that becomes the chasma. However, the deflection caused by the BU reentrant is minor, and most of the wind is still traveling parallel to modern Chasma Boreale even at this early stage. Thus, it is possible that conditions for creating a chasma at this location (by reducing or preventing accumulation) were already in place once BU reworking ceased. An outstanding question, however, is why the large reentrant adjacent to Chasma Boreale was completely filled in by NPLD deposition.

Wind maps created using this paleosurface provide a test for accumulation scenarios pertaining to NPLD and cavi unit. In addition, the modeled winds here offer a direct comparison to modern wind regimes. In that respect, it is interesting to note that the change from present-day topography to BU topography does not drastically alter the wind patterns predicted by mesoscale modeling. It is important to note that local wind variations exist, for example over the now filled reentrant adjacent to Chasma Boreale, but dominantly, there is little change between our simulated ancient winds and the modern winds. This small degree of change in regional wind pattern hints that other factors such as local climatic and atmospheric effects are also significant for NPLD accumulation.

## 6. Conclusions

Detailed radar-derived stratigraphic mapping of Planum Boreum's BU has revealed it to be a highly asymmetric mound of ice- and lithic-rich material containing at least three major reentrant-like features. It is our conclusion that the large-scale asymmetry and the reentrant-like features are erosional in origin, likely occurring at the same geologic time as the major rupes erosion hypothesized by *Tanaka et al.* [2008], and coincident with cavi unit deposition.

The thickest BU is geographically offset from the thickest NPLD and hence offset from the modern depocenter of Planum Boreum. While no explanation for the offset is offered in our work, we do offer

a plausible hypothesis for the creation of the irregular BU morphology, derived solely from katabatic winds and impact ejecta armoring.

To qualitatively investigate the role of winds in forming cavi and NPLD, we modeled paleowinds with a mesoscale atmospheric model and studied the NPLD surface expression above BU reentrants. The BU reentrants deflect and funnel katabatic winds. We suggest that the deflection of winds caused by reentrants has left a signature in modern ice deposits. Ice at each location has aligned series of spiral trough deflections and terminations associated with the outline of the underlying BU reentrant. In addition, these features are concentrated around the BU reentrants; similar features are seldom found elsewhere. As there exists correlation between a unique subsurface topography and modern topography, we hypothesize that the same wind-influenced parameters for ice deposition have been ongoing since the end of rupes unit erosion. This is supported by the extensive geological evidence for aeolian influence in the cavi [*Herkenhoff et al.*, 2007; *Tanaka et al.*, 2008; *Kocurek and Ewing*, 2012]. Further climate modeling, more sophisticated than the simple mesoscale simulation presented in this paper, will be needed to test this hypothesis.

The results of this work emphasize that current Planum Boreum accumulation processes involving the NPLD are very similar, if not the same as, older accumulation processes involving the upper BU. Reentrants exist in both deposits, as do unique morphologies that correlate between the two. Detailed BU mapping has provided new insights into ancient topography that controlled katabatic winds and thus influenced the deposition of water ice on Mars' north pole. The results of this study provide constraints for the evolution of Planum Boreum and hypothesize a regime where wind is the primary force mobilizing and reworking material to generate the modern ice cap starting from the top of the BU.

**Acknowledgments**

This work was supported by NASA grants NNX10AO26G and NNX11AL10G to J.W.H. as well as the MRO Project through a SHARAD Co-I contract to J.W.H. We thank Bruce Campbell for the use of his SHARAD FPB processor and the Southwest Research Institute for use of the boutique SHARAD processor. Data used in this study can be found on the Planetary Data System at http://pds-geosciences.wustl.edu/missions/mro/sharad.htm. Both raw data products and the U.S. SHARAD processor products that were used in this study are stored there. We would also like to thank Kenneth Tanaka and an anonymous reviewer for their helpful reviews of this work.

## References

Arvidson, R. E., M. Coradini, A. Carusi, A. Coradini, M. Fulchignoni, C. Federico, R. Funiciello, and M. Salomone (1976), Latitudinal variation of wind erosion of crater ejecta deposits on Mars, *Icarus*, *27*(4), 503–516, doi:10.1016/0019-1035(76)90166-4.

Brothers, T. C., J. W. Holt, and A. Spiga (2013), Orbital radar, imagery, and atmospheric modeling reveal an aeolian origin for Abalos Mensa, Mars, *Geophys. Res. Lett.*, *40*, 1334–1339, doi:10.1002/grl.50293.

Byrne, S., and B. C. Murray (2002), North polar stratigraphy and the paleo-erg of Mars, *J. Geophys. Res.*, *107*(E6), 11–1, doi:10.1029/2001JE001615.

Campbell, B. A., N. E. Putzig, L. M. Carter, and R. J. Phillips (2011), Autofocus correction of phase distortion effects on SHARAD echoes, *IEEE Geosci. Remote Sens. Lett.*, *8*(5), 939–942, doi:10.1109/LGRS.2011.2143692.

Carter, L. M., et al. (2009), Shallow radar (SHARAD) sounding observations of the Medusae Fossae Formation, Mars, *Icarus*, *199*(2), 295–302, doi:10.1016/j.icarus.2008.10.007.

Christian, S., J. W. Holt, S. Byrne, and K. E. Fishbaugh (2013), Integrating radar stratigraphy with high resolution visible stratigraphy of the north polar layered deposits, Mars, *Icarus*, *226*(2), 1241–1251, doi:10.1016/j.icarus.2013.07.003.

Fishbaugh, K. E., and J. W. Head (2005), Origin and characteristics of the Mars north polar basal unit and implications for polar geologic history, *Icarus*, *174*(2), 444–474, doi:10.1016/j.icarus.2004.06.021.

Forget, F., et al. (2006), The new Mars climate database, in *Second Workshop on Mars Atmosphere Modelling and Observations*, Granada, Spain, 27 Feb.–3 Mar.

Greve, R., B. Grieger, and O. J. Stenzel (2010), MAIC-2, a latitudinal model for the Martian surface temperature, atmospheric water transport and surface glaciation, *Planet. Space Sci.*, *58*(6), 931–940, doi:10.1016/j.pss.2010.03.002.

Grima, C., W. Kofman, J. Mouginot, R. J. Phillips, A. Hérique, D. Biccari, R. Seu, and M. Cutigni (2009), North polar deposits of Mars: Extreme purity of the water ice, *Geophys. Res. Lett.*, *36*, L03203, doi:10.1029/2008GL036326.

Head, J. W., et al. (2005), Tropical to mid-latitude snow and ice accumulation, flow and glaciation on Mars, *Nature*, *434*(7031), 346–351, doi:10.1038/nature03359.

Herkenhoff, K. E., S. Byrne, P. S. Russell, K. E. Fishbaugh, and A. S. McEwen (2007), Meter-scale morphology of the north polar region of Mars, *Science*, *317*(5845), 1711–1715, doi:10.1126/science.1143544.

Holt, J. W., et al. (2008), Radar sounding evidence for buried glaciers in the southern mid-latitudes of Mars, *Science*, *322*(5905), 1235–1238, doi:10.1126/science.1164246.

Holt, J. W., K. E. Fishbaugh, S. Byrne, S. Christian, K. Tanaka, P. S. Russell, K. E. Herkenhoff, A. Safaeinili, N. E. Putzig, and R. J. Phillips (2010), The construction of Chasma Boreale on Mars, *Nature*, *465*(7297), 446–449, doi:10.1038/nature09050.

Howard, A. D. (2000), The role of eolian processes in forming surface features of the Martian polar layered deposits, *Icarus*, *144*(2), 267–288, doi:10.1006/icar.1999.6305.

Kneissl, T., S. Van Gasselt, L. Wendt, C. Gross, and G. Neukum (2011), Layering and degradation of the Rupes Tenuis unit, Mars—A structural analysis south of Chasma Boreale, *Geol. Soc. London Spec. Publ.*, *356*(1), 257–279, doi:10.1144/SP356.13.

Kocurek, G., and R. C. Ewing (2012), Source-to-sink: An Earth/Mars comparison of boundary conditions for eolian dune systems, in *Sedimentary Geology of Mars*, vol. 102, edited by J. Grotzinger and R. Milliken, pp. 151–168, Society for Sedimentary Geology, Tulsa, Okla., doi:10.2110/pec.12.102.0151.

Kolb, E. J., and K. L. Tanaka (2006), Accumulation and erosion of south polar layered deposits in the Promethei Lingula region, Planum Australe, Mars, *Mars*, *2*, 1–9, doi:10.1555/mars.2006.0001.

Laskar, J., A. C. M. Correia, M. Gastineau, F. Joutel, B. Levrard, and P. Robutel (2004), Long term evolution and chaotic diffusion of the insolation quantities of Mars, *Icarus*, *170*(2), 343–364, doi:10.1016/j.icarus.2004.04.005.

Levrard, B., F. Forget, F. Montmessin, and J. Laskar (2007), Recent formation and evolution of northern Martian polar layered deposits as inferred from a global climate model, *J. Geophys. Res.*, *112*(E6), doi:10.1029/2006JE002772.

Madeleine, J.-B., F. Forget, J. W. Head, B. Levrard, F. Montmessin, and E. Millour (2009), Amazonian northern mid-latitude glaciation on Mars: A proposed climate scenario, *Icarus*, *203*(2), 390–405, doi:10.1016/j.icarus.2009.04.037.

Malin, M. C., and K. S. Edgett (2001), Mars Global Surveyor Mars Orbiter Camera: Interplanetary cruise through primary mission, *J. Geophys. Res.*, *106*(E10), 23,429–23,570, doi:10.1029/2000JE001455.

McEwen, A. S., et al. (2007), Mars Reconnaissance Orbiter's High Resolution Imaging Science Experiment (HiRISE), *J. Geophys. Res.*, *112*, E05S02, doi:10.1029/2005JE002605.

Morgan, G. A., B. A. Campbell, L. M. Carter, J. J. Plaut, and R. J. Phillips (2013), 3D reconstruction of the source and scale of buried young flood channels on Mars, *Science*, *340*(6132), 607–610, doi:10.1126/science.1234787.

Phillips, R. J., et al. (2008), Mars north polar deposits: Stratigraphy, age, and geodynamical response, *Science*, *320*(5880), 1182–1185, doi:10.1126/science.1157546.

Picardi, G., et al. (2004), MARSIS: Mars Advanced Radar for Subsurface and Ionosphere Sounding, in *Mars Express: A European Mission to the Red Planet*, *ESA Report SP-1240*, edited by A. Wilson, pp. 51–69, European Space Agency Publ. Division, ESTEC, Noordwijk, Netherlands, Paris, France.

Putzig, N. E., R. J. Phillips, B. A. Campbell, J. W. Holt, J. J. Plaut, L. M. Carter, A. F. Egan, F. Bernardini, A. Safaeinili, and R. Seu (2009), Subsurface structure of Planum Boreum from Mars Reconnaissance Orbiter shallow radar soundings, *Icarus*, *204*(2), 443–457.

Russell, P., et al. (2008), Seasonally active frost-dust avalanches on a north polar scarp of Mars captured by HiRISE, *Geophys. Res. Lett.*, *35*, L23204, doi:10.1029/2008GL035790.

Selvans, M. M., J. J. Plaut, O. Aharonson, and A. Safaeinili (2010), Internal structure of Planum Boreum, from Mars Advanced Radar for Subsurface and Ionospheric Sounding data, *J. Geophys. Res.*, *115*, E09003, doi:10.1029/2009JE003537.

Seu, R., et al. (2007), SHARAD sounding radar on the Mars Reconnaissance Orbiter, *J. Geophys. Res.*, *112*(E5), 1715–1718, doi:10.1029/2006JE002745.

Sibson, R. (1981), A brief description of natural neighbour interpolation, in *Interpreting Multivariate Data*, pp. 21–36, John Wiley, New York.

Smith, D. E., et al. (2001), Mars Orbiter Laser Altimeter: Experiment summary after the first year of global mapping of Mars, *J. Geophys. Res.*, *106*(E10), 23,689–23,722, doi:10.1029/2000JE001364.

Smith, I. B., and J. W. Holt (2010), Onset and migration of spiral troughs on Mars revealed by orbital radar, *Nature*, *465*(7297), 450–453, doi:10.1038/nature09049.

Smith, I. B., and J. W. Holt (2015), Spiral trough diversity on the north pole of Mars, as seen by SHARAD, *J. Geophys. Res. Planets*, *120*, 362–387, doi:10.1002/2014JE004720.

Smith, I. B., J. W. Holt, A. Spiga, A. D. Howard, and G. Parker (2013), The spiral troughs of Mars as cyclic steps, *J. Geophys. Res. Planets*, *118*, 1835–1857, doi:10.1002/jgre.20142.

Spiga, A., and F. Forget (2009), A new model to simulate the Martian mesoscale and microscale atmospheric circulation: Validation and first results, *J. Geophys. Res.*, *114*, E02009, doi:10.1029/2008JE003242.

Spiga, A., F. Forget, J.-B. Madeleine, L. Montabone, S. R. Lewis, and E. Millour (2011), The impact of Martian mesoscale winds on surface temperature and on the determination of thermal inertia, *Icarus*, *212*(2), 504–519, doi:10.1016/j.icarus.2011.02.001.

Tanaka, K., J. Rodriguez, J. Skinner, M. Bourke, C. Fortezzo, K. Herkenhoff, E. Kolb, and C. Okubo (2008), North polar region of Mars: Advances in stratigraphy, structure, and erosional modification, *Icarus*, *196*(2), 318–358, doi:10.1016/j.icarus.2008.01.021.

Tanaka, K. L., and C. M. Fortezzo (2012), Geologic map of the north polar region of Mars, *U.S. Geol. Surv. Sci. Invest.*, *Map 3177*.

Tanaka, K. L., and R. K. Hayward (2008), Mars' north circum-polar dunes: Distribution, sources, and migration history, in *Planetar Dunes Workshop: A Record of Climate Change*, *LPI Contribution No. 1403*, pp. 69–70, Lunar and Planetary Inst., Houston, Tex.

Warner, N. H., and J. D. Farmer (2008a), Importance of aeolian processes in the origin of the north polar chasmata, Mars, *Icarus*, *196*(2), 368–384, doi:10.1016/j.icarus.2007.08.043.

Warner, N. H., and J. D. Farmer (2008b), The origin of conical mounds at the mouth of Chasma Boreale, *J. Geophys. Res.*, *113*, E11008, doi:10.1029/2007JE003028.

Zurek, R. W., and S. E. Smrekar (2007), An overview of the Mars Reconnaissance Orbiter (MRO) science mission, *J. Geophys. Res.*, *112*, E05S01, doi:10.1029/2006JE002701.